WILEY-VCH

Shiao-Wei Kuo

Hydrogen Bonding in Polymeric Materials

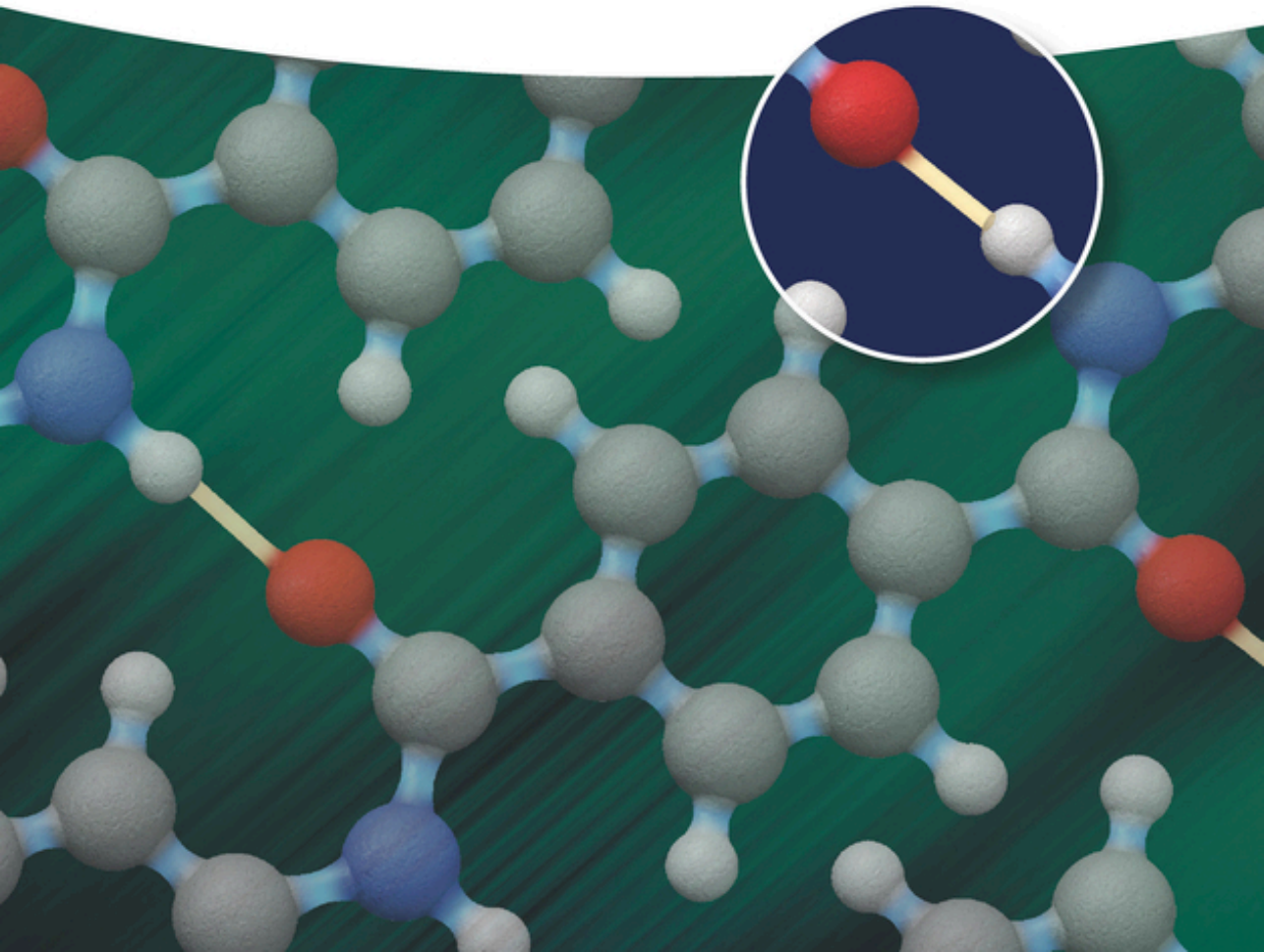

Hydrogen Bonding in Polymer Materials

Hydrogen Bonding in Polymer Materials

Shiao-Wei Kuo

WILEY-VCH

Author

Prof. Shiao-Wei Kuo
National Sun Yat-Sen University
Department of Materials and
Optoelectronics
No. 70 Lienhai Rd.
80424 Kaohsiung
Taiwan

Cover
(Foreground image) © theasis/
Gettyimages
(Background image) © ricardoreitmeyer/
Gettyimages

Library of Congress Card No.: applied for

British Library Cataloguing-in-Publication Data
A catalogue record for this book is available from the British Library.

Bibliographic information published by the Deutsche Nationalbibliothek
The Deutsche Nationalbibliothek lists this publication in the Deutsche Nationalbibliografie; detailed bibliographic data are available on the Internet at <http://dnb.d-nb.de>.

Print ISBN: 978-3-527-34188-7
ePDF ISBN: 978-3-527-80426-9
ePub ISBN: 978-3-527-80428-3
Mobi ISBN: 978-3-527-80429-0
oBook ISBN: 978-3-527-80427-6

Typesetting Spi Global, Chennai, India
Printing and Binding

Printed on acid-free paper

10 9 8 7 6 5 4 3 2 1

Contents

Preface

I dedicate this book to my advisor, Professor Feng-Chih Chang, who strongly encouraged its writing about 10 years ago. At that time, I had just left his group to start my research career independently at National Sun Yat-Sen University. Since then, every time we met in his office we would discuss writing a book together about hydrogen bonding in polymeric materials, and we had assembled a rough outline of its contents. Unfortunately, Professor Chang passed away in 2014. I began to pay serious attention to this project in 2015, when Wiley invited me to publish a book about supramolecular interactions—quite close to our original concept. Although only some of the results described in this book were published independently by Professor Chang's group, I feel it is appropriate to say "our group" herein to appreciate his great contributions to this field.

In 1998, I entered Professor Chang's group and began investigating hydrogen bonding interactions in polymer blend systems. Our group was the first to publish several important findings in the field at around that time. Chapter 1 provides an introduction to the nature of hydrogen bonds and describes several methods (including Fourier transform infrared (FTIR) and nuclear magnetic resonance (NMR) spectroscopy) for characterizing them. Chapter 2 discusses the factors that influence hydrogen bonding in polymer blend systems, how to determine their thermodynamic properties (including use of the association model approach), and how to enhance the miscibility of polymer blends through hydrogen bonding. Chapter 3 describes the physical properties of polymeric materials capable of hydrogen bonding, including their thermal properties, dynamic behavior, and crystalline structures. Chapter 4 discusses the surface properties of polymeric materials. In 2006, we were the first to develop polybenzoxazine, a fluorine- and silicone-free polymer, that has a low surface free energy as a result of strong intramolecular hydrogen bonds; PVPh is another polymeric material having a low surface free energy, this time arising from both inter- and intramolecular hydrogen bonds. This chapter also describes the potential applications of low surface free energy polymers, including their use in nanoimprint technologies and as superhydrophobic surfaces. Chapter 5 considers the sequence distribution effects found in hydrogen-bonded copolymers, including random copolymers, block copolymers, and polymer blend systems.

Chapter 6 describes the properties, in the bulk and in solution, of block copolymer mixtures that form self-assembled structures stabilized through hydrogen bonding interactions. Chapter 7 reports the preparation of

mesoporous materials—particularly mesoporous silica and phenolic and carbon materials—self-assembled, primarily through hydrogen bonding, from block copolymer/homopolymer blends. Chapter 8 discusses the behavior of two types of bioinspired macromolecules—polypeptides and DNA-like polymers—that have properties dependent on their hydrogen bonding interactions. Polypeptides prepared from polymer blends and block copolymers form interesting secondary and self-assembled structures; DNA-like polymers are materials featuring multiple hydrogen bonding interactions. Finally, Chapter 9 focuses on hydrogen bonding in POSS nanocomposites, the properties of which are also strongly influenced by inter- and intramolecular interactions.

Herein, I acknowledge several important works that are described in this book from more than 100 graduate students in Professor Chang's group in National Chiao-Tung University and my group in National Sun Yat-Sen University. Those students worked hard on the hydrogen bonding in polymeric materials. I hope this book is not only useful to the reader but also enjoyable to read. Understanding hydrogen bonding is of fundamental importance to chemists, physicists, and materials scientists. I will be honored if this book inspires its readers to apply some of the concepts of hydrogen bonding to their own research—or, even better, develop new ones not yet explored.

National Sun Yat-Sen University, Taiwan *Shiao-Wei Kuo*
August 2017

Abbreviation

2D-FTIR	two-dimensional Fourier transform infrared
A	adenine
ACA	vinyl alcohol-*co*-vinyl acetate
AFM	atomic force microscopy
AIBN	azoisobutyronitrile
AIM	attractive interaction model
A-PCL	adenine-terminated three-arm PCL oligomer
A-PEO	adenine-terminated PEO
A-PS	PS-*co*-PVBA
A-PTC	A-functionalized poly(triphenylamine-*co*-carbazole)
ATP	adenosine triphosphate
ATRP	atom transfer radical polymerization
Azo-COOH BZ	azo-carboxylic acid-benzoxazine
AzoPy-BZ	azopyridine-benzoxazine
Azo-T	T-functionalized azobenzene
BA-a	bisphenol A-aniline
B-ala	bisphenol A-allylamine
BA-m	bisphenol A-methylamine
BA-PC	bisphenol-A polycarbonate
BCC	body-centered cubic
BPA	bisphenol A
C	cytosine
CA	contact angle
CD	circular dichroism
CHEX	cyclohexane
CNT	carbon nanotube
COC	cyclic olefin copolymer
CPB	carboxyl-terminated polybutadiene
C&S	Coggeshall and Saier
CPC	cetylpyridinium chloride
CPS	carboxyl-terminated polystyrene
CTAB	cetyltrimethylammonium bromide
CVD	chemical vapor deposition
DAN	2,7-diamido-1,8-naphthyridine
DAP	diaminopyridine

DAT	diamino-triazine
DDA	dodecanedioic acid
DDSQ	double-deckered silsesquioxanes
DI	diiodomethane
DMA	dynamic mechanic analysis
DMF	dimethylformamide
DMP	dimethyl phenol
DOX	doxorubicin hydrochloride
DP	degree of polymerization
D-PMMA	poly(methyl methacrylate-*co*-2-vinyl-4,6-diamino-1, 3,5-triazine)
DSC	differential scanning calorimetry
EG	ethylene glycol
EIAA	evaporation-induced aggregation assembly
EISA	evaporation-induced self-assembly
EMAA	ethylene-*co*-methacrylic acid
EPr	ethyl pyrrolidone
FA	formic acid
FCC	face-centered cubic
FFT	fast Fourier transform
FIC	fluorescein isothiocyanate
FTIR	Fourier transform infrared
G	guanine
H-bond	hydrogen bond
HEC	hydroxyethyl cellulose
HITL	hole injection/transport material
HMTA	hexamethylenetetramine
IPP	4-isopropyl phenol
K_2	self-association equilibrium constant of dimers
K_A	interassociation equilibrium constant with A homopolymer
K_B	self-association equilibrium constant of multimers
K_C	interassociation equilibrium constant with C homopolymer
LCST	lower critical solution temperature
LCT	liquid crystal templating
LED	light emitting diode
$LiClO_4$	lithium perchlorate
LMC	low-molecular-weight compound
MALDI-TOF	matrix-assisted laser desorption inoization-time of flight
MA-POSS	methacrylic POSS
MIPOSS	melaimide-POSS
MMT	montmorillonite
NCA	*N*-carboxyanhydride
NCCM	noncovalently connected micelles
NDP	nonadecylphenol
NIL	nanoimprint lithography
NMR	nuclear magnetic resonance
NMRP	nitroxide-mediated radical polymerization

NPs	nanoparticles
OA-POSS	octakis[dimethyl(4-acetoxy phenethyl)siloxy]-POSS
OAc-POSS	octa-functionalized acrylate POSS
OAM-POSS	octakis(dimethylsiloxy-aminopropyl)-POSS
OAP-POSS	octakis(dimethylsiloxy-aminophenyl)-POSS
OBA-POSS	octa-functionalized adenine (A)-POSS
OBZ-POSS	octa-functionalized BZ POSS
OcapPOSS	OAP-POSS with cinnamoyl chloride
OF-POSS	octakis(dimethylsiloxy-hexafluoropropyl ether)-POSS
OG	octyl gallate
OG-POSS	octakis(glycidyl dimethylsilyl)-POSS
OH-POSS	octakis(3-hydroxypropyldimethylsilyl)-POSS
OLED	organic light-emitting device
OM	optical microscopy
OP-POSS	octakis[dimethyl(4-hydroxyphenethyl)siloxy]-POSS
OS-POSS	octakis[dimethyl(phenethyl)siloxy]-POSS
OTFT	organic thin-film transistor
OT-POSS	octa-functionalized *N*-alkoxyamine POSS
OVBC-POSS	octa-functionalized vinyl benzyl chloride POSS
$OVBN_3$-POSS	octa-azido functionalized polyhedral oligomeric silsesquioxane
OV-POSS	octa-vinyl POSS
P2VP	poly(2-vinyl pyridine)
P3HT	poly(3-hexylthiophene)
P4VP	poly(4-vinyl pyridine)
P-a	phenol-aniline
PA6	nylon 6 or poly(caprolactam)
PAA	poly(acrylic acid)
PAA	poly(amic acid), precursor of polyimide
PALa	polyalanine
PAMA	poly(*n*-alkyl methacrylate)
PAN	poly(acrylonitrile)
PAS	poly(acetoxystyrene)
PA-T	T-functionalized BZ
PAT	A-functionalized P3HT
PB	poly(butadiene)
PBLG	poly(γ-benzyl-L-glutamate)
PBMA	poly(butyl methacrylate)
PBPMA	poly(bromophenyl methacrylamide)
PBSA	poly(butylene succinate-*co*-adipate)
PBT	poly(butylene terephthalate)
PBZ	polybenzoxazine
PBzMA	poly(benzyl methacrylate)
PC	poly(carbonate)
PCAM	Painter–Coleman association model
PCHMA	poly(cylcohexyl methacrylate)
PCL	poly(caprolactone)

PDA	poly(adipic ester)
PDEMA	poly[2-(dimethylamino)ethyl methacrylate]
PDMA	poly(*N*,*N*-dimethylacrylamide)
PDMS	poly(dimethylsiloxane)
PDP	pentadecyl phenol
PE	poly(ethylene)
PECH	poly(epichlorohydrin)
PEDEK	poly(ether diphnyl ether ketone)
PEDOT/PSS	poly(3,4-ethylenedioxythiophene)/polystyrene sulfonate
PEEK	poly(ether ether ketone)
$P(EG_2LG)$	poly(*r*-(2-methoxyethoxy)esteryl-L-glutamate)
PEI	poly(ether imine)
PELG	poly(γ-ethyl-L-glutamate)
PEMA	poly(ethyl methacrylate)
PET	poly(ethylene terephthalate)
PEO	poly(ethylene oxide)
PEOx	poly(2-ethyl-2-oxazoline)
PEPS	poly(4-ethenylphenolmethylsiloxane)
PF	polyfluorene
PHB	poly(hydroxybutyrate)
PHEMA	poly(hydroxylethyl methacraylte)
PHPMA	poly(hydroxylpropyl methacrylate)
PI	poly(isoprene)
PI	polyimide
PL	photoluminescence
PLA	poly(D,L-lactic acid)
PLED	polymer light-emitting device
PLLA	poly(L-lactic acid)
PLys	poly(*Z*-L-lysine)
PMA	poly(methyl acrylate)
PMAA	poly(methylacrylic acid)
PMAAM	poly(methyl methacrylamide)
PMLG	poly(γ-methyl-L-glutamate)
PMMA	poly(methyl methacrylate)
PMPMA	poly(methoxyphenyl methacrylamide)
PMPMA	poly(*N*-methyl-3-piperidinemethyl methacrylate)
PNCHMA	poly(cyclohexyl methacrylamide)
PNIPAAm	poly(*N*-isopropyl acrylamide)
PNMAA	poly(methyl methacrylamide)
PNPAA	poly(phenyl methacrylamide)
Poly(TFP-tmos)	4-trifluoremethylphenol-3-aminopropyltrimethoxysilane
POSS	polyhedral oligomeric silsesquioxanes
P-pa	phenol-propargylamine
PPLG	poly(γ-propargyl-L-glutamate)
PPLG-DAP	PPLG functionalized with diaminopyridine
PPO	poly(phenyl oxide)
PPzMA	poly(phenyl methacrylate)

PS	poly(styrene)
PSOH	poly(styrene-*co*-vinyl phenol)
PtBMA	poly(*t*-butyl methacrylate)
PTC	poly(triphenylamine-*co*-carbazole)
PTFE	poly(tetrafluoroethylene)
PTyr	polytyrosine
PVA	poly(vinyl alcohol)
PVAc	poly(vinyl acetate)
PVBA	poly(vinyl benzyl adenine)
$PVBN_3$	poly(vinyl benzyl azido)
PVBT	poly(vinylbenzyl)thymine
PVC	poly(vinyl chloride)
PVDAT	poly(2-vinyl-4,6-diamino-1,3,5-triazine)
PVDF	poly(vinylidene fluoride)
PVME	poly(vinyl methyl ether)
PVP	poly(vinyl pyrrolidone)
PVPh	poly(vinyl phenol)
PVPK	poly(vinyl phenyl ketone)
Py-A	A-functionalized pyrene
Py-Bz-T	thymine and pyrene-functionalized benzoxazine
Py-T	T-functionalized pyrene
$Q_8M_8{}^H$	octakis(dimethylsiloxy)silsesquioxane
RIE	reactive ion etching
ROP	ring-opening polymerization
SAA	styrene-*co*-acrylic acid
SAED	selective area electron diffraction
SAN	styrene-*co*-acrylonitrile
SAXS	small-angle X-ray scattering
SBA	suberic acid
SCA	succinic acid
SEM	scanning electron microscopy
SH-POSS	mercaptopropyl-isobutyl-POSS
SLS	static light scattering
suPI	sulfonic acid end-capped poly(isoprene)
SWCNT	single-walled carbon nanotube
T	thymine
T_1(H)	spin–lattice relaxation time
TAc	4-tolyl acetate
T-C16	hexadecylthymine
TEM	transmission electron microscopy
TEOS	tetraethyl orthosilicate
T_f	freezing temperatures
T_g	glass transition temperature
TGA	thermal gravity analysis
THF	tetrahydrofuran
T_m	melting temperature
TM-PC	tetramethyl bisphenol-polycarbonate

T_{ODT}	order–disorder temperature
T-PBMA	PBMA-*co*-PVBT
T-PMMA	PMMA-*co*-PVBT
U-POSS	multi-uracil functionalized POSS
U-PTC	U-functionalized poly(triphenylamine-*co*-carbazole)
UPy	2-ureido-4[1*H*]-pyrimidinone
UPyMA	2-ureido-4-pyrimidinone methyl methacrylate
UV	ultraviolet
VBA	vinyl benzyl adenine
VBT	vinyl benzyl thymine
VDAT	2-vinyl-4,6-diamino-1,3,5-triazine
WAXD	wide-angle X-ray diffraction
XPS	X-ray photoelectron spectroscopy

1

Hydrogen Bonding in Polymeric Materials

1.1 Introduction

Hydrogen-bonding, dipole–dipole, and ionic interactions in polymers have been of great interest to fundamental polymer science, and also industrially, for over 30 years. These secondary or noncovalent interactions can be introduced specifically into polymeric materials to form supramolecular materials displaying interesting thermal, mechanical, surface, and optoelectronic properties. The concept of noncovalent bonding has changed the thinking of polymer scientists, who had been focused for many years primarily on the effects of covalent interactions.

Hydrogen bonds (H-bonds) are interactions that result from dipole–dipole forces between strongly electronegative atoms (e.g., fluorine (F), nitrogen (N), oxygen (O)), and hydrogen atoms; they affect the physical properties and microstructures of many materials [1–6]. For example, water is recognized to form tetrahedral clusters comprising 14 molecules of H_2O; the unusual properties of water arise mainly from the fact that water molecules readily form H-bonds—4 of them—per water molecule, in a tetrahedral geometry [7]. Other famous examples are the H-bonds found in biological systems [8], where they play important roles affecting the three-dimensional structures of nucleic bases and proteins. The DNA double helix is formed from multiple H-bonding interactions between complementary cytosine/guanine (C/G) and adenine/thymine (A/T) base pairs; these noncovalent interactions link the two complementary strands and enable replication. Furthermore, H-bonds greatly influence the secondary structures of polypeptides: the α-helix conformation is stabilized by intramolecular (or intrachain) H-bonding, while the β-sheet conformation is stabilized by intermolecular (or interchain) H-bonding [9, 10]. In addition to these famous natural examples, H-bonding also has several profound effects in unnatural polymeric materials, influencing various physical, thermal, and mechanical properties, including melting points (T_m), crystalline structures, glass transition temperatures (T_g), surface properties, optoelectronic properties, and solubilities (in solvents) and miscibilities (in polymer blends).

Although there are already several reviews on H-bonded polymer blends, copolymers, self-assembled supramolecular structures, and nanocomposite systems [11–21], this book aims to provide a thorough discussion of how H-bonding interactions have been used in research into polymer blends, surface properties,

Hydrogen Bonding in Polymer Materials, First Edition. Shiao-Wei Kuo.

self-assembled block copolymers, mesoporous materials, biomacromolecules, and polyhedral oligomeric silsesquioxanes (POSS) nanocomposites.

1.1.1 Hydrogen Bonds

Hydrogen bonding is a fundamental interaction in chemistry, physics, and biology and has been described extensively in many books [22] and reviews [23]. The H-bond is a directed, attractive, noncovalent bonding interaction between an A–H unit (proton donor) and a B atom (proton acceptor) in the same molecule or in different molecules, where the A and B atoms are generally highly electronegative (e.g., F, N, O), although even C–H groups can be involved in H-bonding and some π-electrons can act as weak H-bond acceptors [24, 25]. The H-bond can also be characterized by its effect on the physical properties or molecular characteristics of a material. A covalent bond usually has strength on the order of 50 kcal mol^{-1}; H-bonds most often have stabilities in the range 1–40 kcal mol^{-1} (in comparison, van der Waals attraction is favorable by only approximately 0.2 kcal mol^{-1}). A strong H-bond has strength in the range 10–40 kcal mol^{-1}; a moderate H-bond, 4–10 kcal mol^{-1}; and a weak H-bond, 1–4 kcal mol^{-1} [26].

Hydrogen bonding can be either an intermolecular or intramolecular phenomenon. An intermolecular H-bond (Figure 1.1) is one for which the donor and acceptor units are found in two different molecules; for an intramolecular H-bond (Figure 1.2) they are in the same molecule. Intermolecular H-bonds are usually linear or near linear, whereas intramolecular H-bonds usually feature some degree of bending. In polymers, two different types of H-bonding can occur for the same functional group, namely, interchain and intrachain H-bonding interactions. For example, the α-helix conformation of a polypeptide is stabilized by intrachain H-bonding, while the β-sheet conformation is stabilized by interchain H-bonding. The strength of an H-bond is strongly dependent on the solvent polarity; the addition of a polar solvent can decrease the H-bond

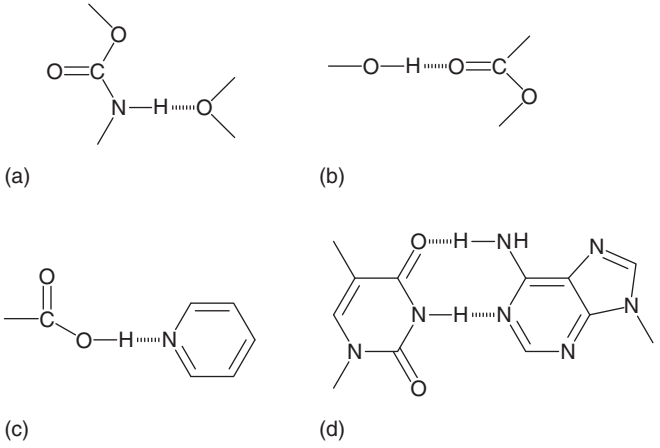

Figure 1.1 Intermolecular H-bonding between two molecules. (a) Urethane–ether complex; (b) hydroxyl–carbonyl complex; (c) acid–pyridine complex; and (d) adenine–thymine complex.

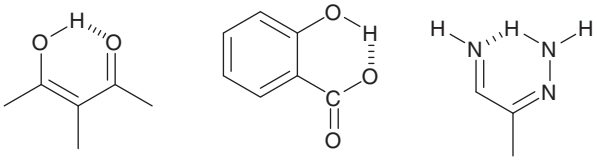

Figure 1.2 Intramolecular H-bonding of a single molecule. (a) Malonaldehyde; (b) salicyclic acid; and (c) formazan.

strength significantly, over several orders of magnitude, because the solvent molecule can also take part in H-bonding interactions. As a result, nonpolar solvents (e.g., toluene, $CHCl_3$, and linear and cyclic alkanes) are mostly used for the preparation of H-bonded supramolecular materials.

1.1.2 Characterization of Hydrogen Bonding

Several spectroscopic methods are commonly used to characterize H-bonds: (i) Fourier transform infrared (FTIR) and Raman spectroscopy, in which the stretching and bending vibrations of the donor or acceptor functional groups are influenced by the presence of H-bonds; (ii) ultraviolet (UV) and fluorescence spectroscopy, which reveal changes in the electronic levels of molecules experiencing H-bond interactions; (iii) nuclear magnetic resonance (NMR) spectroscopy, where changes in chemical shifts can arise from H-bond interactions of the donor and acceptor functional groups; and (iv) X-ray photoelectron (XPS) spectroscopy, where a new shoulder or even a new peak can appear as a result of a change in the chemical environment of an atom perturbed by the H-bonding [27–30].

Among these methods for characterizing H-bonds, by far the most inexpensive and sensitive is FTIR spectroscopy. For example, Figure 1.3 presents the CO stretching range of the FTIR spectra of H-bonded phenolic/PCL blends of various compositions. The signal for C=O stretching in this phenolic/PCL blend splits into two bands: a signal at higher wavenumber (1734 cm^{-1}) corresponding to the free C=O groups of PCL, and one at relatively lower wavenumber (1708 cm^{-1}) representing the C=O groups of PCL H-bonded with phenolic OH groups. If we can resolve these peaks into two Gaussian functions, we can quantify the fraction of H-bonded C=O groups using the appropriate absorptivity ratio between the two peaks. Using this approach, we can see that the fraction of H-bonded C=O groups of PCL increased upon increasing the content of phenolic in the blend [31].

In addition to one-dimensional (1D) infrared (IR) spectra (e.g., in Figure 1.3), two-dimensional (2D) correlation spectroscopy can also be used to characterize H-bonding interactions in polymer materials [32–34]. Through measurements of spectral perturbations in response to temperature, time, composition, or pressure, we can identify inter- or intramolecular H-bond interactions through analyses of the selected bands based on the corresponding 1D infrared spectra. Figure 1.4 displays a typical 2D-IR correlation spectrum of PVPh/PVPK blends in the region 1500–1700 cm^{-1} [35]. The spectrum features two independent axes

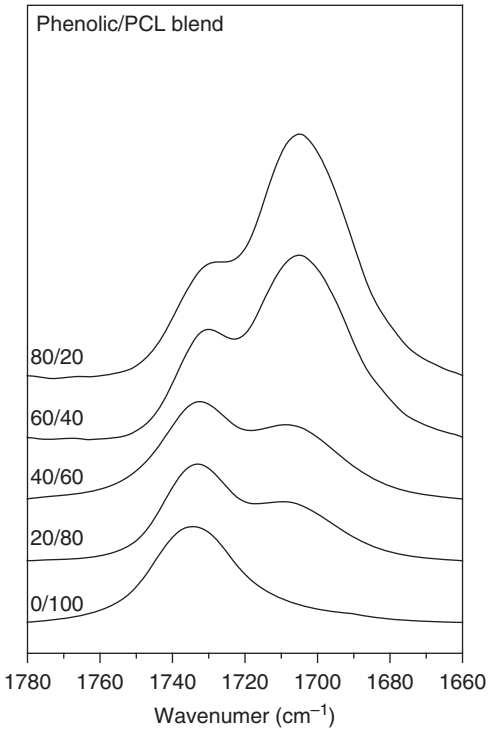

Figure 1.3 Typical infrared (IR) spectra, displaying the C=O stretching region, of phenolic/PCL blends.

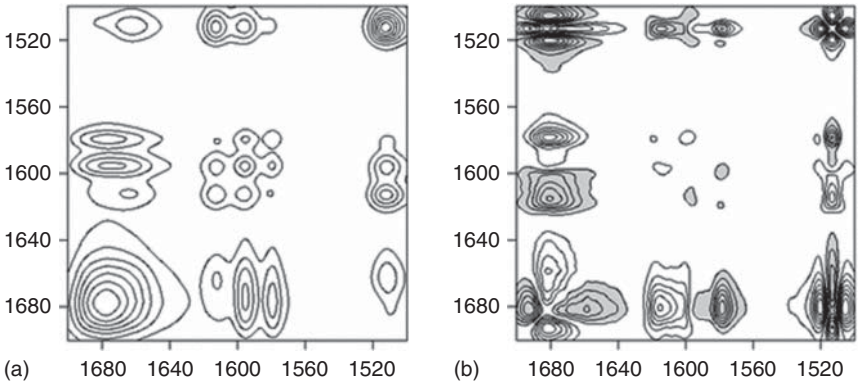

Figure 1.4 2D Fourier transform infrared (FTIR) correlation maps of PVPh/PVPK blends: (a) synchronous and (b) asynchronous maps [35].

for the wavenumber, as well as the correlation intensity. White and shadowed areas represent positive and negative cross-peaks, respectively, in the 2D contour maps. Two types of 2D correlation spectra are generally obtained: synchronous spectra (Figure 1.4a), in which the correlation intensity indicates the relative in-phase degree, and asynchronous spectra (Figure 1.4b), in which the correlation intensity indicates the relative out-of-phase degree. The correlation map in the 2D synchronous spectrum in Figure 1.4a was symmetrical corresponding

to the diagonal line. These intensities of auto-peaks in 2D synchronous spectra should be positive when located at the diagonal line, corresponding to the autocorrelation degree from perturbation-induced molecular vibration. The cross-peaks in 2D synchronous spectra may possess positive (white) or negative (shadow) intensities, corresponding to simultaneous and coincidental changes in the variations of the correlation intensities measured at off-diagonal positions for two different wavenumbers (ν_1, ν_2). A positive cross-peak results when the changes in the signals at these two wavenumbers (ν_1, ν_2) occur in the same direction under the environmental perturbation (i.e., both increase or both decrease). If the signals at the two wavenumbers (ν_1, ν_2) change in opposite directions under the environmental perturbation (i.e., one decreases while the other increases), a negative cross-peak will appear. The asynchronous cross-peaks can also be either positive or negative, giving sequential order information for the external variable. Figure 1.4b displays the asymmetric 2D asynchronous spectrum corresponding to the diagonal line.

Figure 1.4a reveals positive cross-peaks for the correlation intensity of the signal at 1680 cm^{-1} with those at 1612 and 1510 cm^{-1}, implying intermolecular H-bonding between the phenolic OH groups of PVPh (1612 and 1510 cm^{-1}) and the C=O groups of PVPK (1680 cm^{-1}), with changes in the same direction. It also reveals positive cross-peaks between the signals at 1612 cm^{-1} (PVPh) and 1580 cm^{-1} (PVPK), implying π–π interactions among the aromatic rings of PVPh and PVPK, again in the same direction. As a result, the intermolecular interactions in PVPh/PVPK blends arise not only from intermolecular OH···O=C H-bonding but also from π–π interactions of the aromatic rings. Figure 1.4b displays the 2D asynchronous spectrum of the PVPh/PVPK blend. The positive peaks at (1580, 1612 cm^{-1}), (1612, 1680 cm^{-1}), and (1680, 1580 cm^{-1}) imply that the sequence of order in the spectra is 1612 > 1680 > 1580 cm^{-1}, based on the changes in intensity of these three observed bands according to Noda's rule [36].

Solid-state NMR spectroscopy can also provide useful information for identifying H-bonding, by observing the line shapes or chemical shifts in the spectra that are sensitive to the local chemical environment. Figure 1.5 provides an example of this chemical shift in the ^{13}C solid-state NMR spectra of a phenolic/PVAc binary blend [37]. Downfield chemical shifts occurred for the signals of the C=O groups of PVAc (by about 3 ppm) and the OH-substituted carbon atoms in the phenolic resin (by about 2.3 ppm), implying that the H-bonding interactions existed in the phenolic/PVAc blend. The chemical environments of neighboring nuclei can also be influenced by H-bonding in polymer blend systems, leading to downfield chemical shifts that are widely used to provide evidence for H-bonding in polymer blend systems. In addition, the C=O units in the ^{13}C solid-state NMR spectra were also resolved into two peaks—similar to the situation in FTIR spectra (cf. Figure 1.3)—that represented the free (high field at about 171 ppm) and H-bonded (downfield at about 174 ppm) C=O groups of PVAc. The fraction of H-bonded C=O groups of PVAc increased upon increasing the concentration of phenolic resin, similar to the observation in the FTIR spectroscopic analysis. Solid-state NMR spectroscopy can also provide evidence for the miscibility scale of H-bonded polymer blend systems, determined from the proton spin–lattice relaxation time [T_1(H)] [38–40]; a single, composition-dependent value of T_1(H)

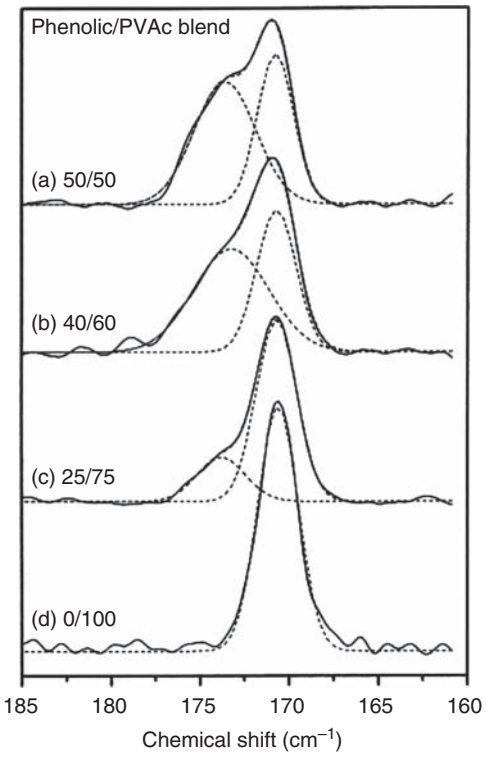

Figure 1.5 Solid-state nuclear magnetic resonance (NMR) spectra and corresponding curve-fitting results for phenolic/PVAc blends [37].

in a polymer blend system represents a homogeneous amorphous phase to the scale by the spin diffusion within the time occurring.

References

1 Errera, J. and Mollet, P. (1936) Intermolecular forces and O—H absorption bands in alcohols at 3. *Nature*, **138**, 882.

2 Etter, M.C. (1990) Encoding and decoding hydrogen-bond patterns of organic compounds. *Acc. Chem. Res.*, **23**, 120–126.

3 Schwager, F., Marand, E., and Davis, R.M. (1996) Determination of self-association equilibrium constants of ethanol by FTIR spectroscopy. *J. Phys. Chem.*, **100**, 19268–19272.

4 Bereo, M., Ikeshoji, T., Liew, C.C., Terakura, K., and Parinello, M. (2004) Hydrogen bond driven chemical reactions: Beckmann rearrangement of cyclo-hexanone xxime into ε-caprolactam in supercritical water. *J. Am. Chem. Soc.*, **126**, 6280–6286.

5 Parmar, D., Sugiono, E., Raja, S., and Rueping, M. (2014) Complete field guide to asymmetric BINOL-phosphate derived Brønsted acid and metalcatalysis: History and classification by mode of activation; Brønsted acidity, hydrogen bonding, ion pairing, and metal phosphates. *Chem. Rev.*, **114**, 9047–9153.

6 Jones, W.D. (2000) Conquering the carbon–hydrogen bond. *Science*, **287**, 1942–1943.

7 Fecko, C.J., Eaves, J.D., Loparo, J.J., Tokmakoff, A., and Geissler, P.L. (2003) Ultrafast hydrogen-bond dynamics in the infrared spectroscopy of water. *Science*, **301**, 1698–1702.

8 Watson, F.P. and Crick, F.H. (1953) Genetical implications of the structure of deoxyribonucleic acid. *Nature*, **171**, 964–967.

9 Pauling, L., Corey, R.B., and Branson, H.R. (1951) The structure of proteins: two hydrogen-bonded helical configurations of the polypeptide chain. *Proc. Natl. Acad. Sci. U.S.A.*, **37**, 205–211.

10 Pauling, L. and Corey, R.B. (1951) Configurations of polypeptide chains with favored orientations around single bonds two new pleated sheets. *Proc. Natl. Acad. Sci. U.S.A.*, **37**, 729–740.

11 Coleman, M.M. and Painter, P.C. (1995) Hydrogen bonded polymer blends. *Prog. Polym. Sci.*, **20**, 1–59.

12 Jiang, M., Mei, L., Xiang, M., and Zhou, H. (1999) Interpolymer complexation and miscibility enhancement by hydrogen bonding. *Adv. Polym. Sci.*, **146**, 121–196.

13 He, Y., Zhu, B., and Inoue, Y. (2004) Hydrogen bonds in polymer blends. *Prog. Polym. Sci.*, **29**, 1021–1051.

14 Binder, W.H. and Zirbs, R. (2007) Supramolecular polymers and networks with hydrogen bonds in the main-and side-chain. *Adv. Polym. Sci.*, **207**, 1–78.

15 Bouteiller, L. (2007) Assembly via hydrogen bonds of low molar mass compounds into supramolecular polymers. *Adv. Polym. Sci.*, **207**, 79–112.

16 ten Brinke, G., Ruokolaine, J., and Ikkala, O. (2007) Supramolecular materials based on hydrogen-bonded polymers. *Adv. Polym. Sci.*, **207**, 113–178.

17 Xu, H., Srivastave, S., and Rotello, V.M. (2007) Nanocomposites based on hydrogen bonds. *Adv. Polym. Sci.*, **207**, 179–198.

18 Kuo, S.W. (2008) Hydrogen-bonding in polymer blends. *J. Polym. Res.*, **15**, 459–486.

19 Fox, J.D. and Rowan, S.J. (2009) Supramolecular polymerizations and main-chain supramolecular polymers. *Macromolecules*, **42**, 6823–6835.

20 Huang, S.H., Chiang, Y.W., and Hong, J.L. (2015) Luminescent polymers and blends with hydrogen bond interactions. *Polym. Chem.*, **6**, 497–508.

21 Voorhaar, L. and Hoogenboom, R. (2016) Supramolecular polymer networks: hydrogels and bulk materials. *Chem. Soc. Rev.*, **45**, 4013–4031.

22 Jeffrey, G.A. and Saenger, W. (1991) *Hydrogen Bonding in Biological Structures*, Springer, Berlin, Heidelberg, New York.

23 Calhorda, M.J. (2000) Weak hydrogen bonds: theoretical studies. *Chem. Commun.*, 801–809.

24 Kuo, S.W., Huang, W.J., Huang, C.F., Chan, S.C., and Chang, F.C. (2004) Miscibility, specific interactions, and spherulite growth rates of binary poly (acetoxystyrene)/poly (ethylene oxide) blends. *Macromolecules*, **37**, 4164–4173.

25 Kuo, S.W., Huang, C.F., Tung, P.H., Huang, W., Huagn, J., Chang, J.M., and Chang, F. (2005) Synthesis, thermal properties, and specific interactions of

high T_g increase in poly (2,6-dimethyl-1,4-phenylene oxide)-block-polystyrene copolymers. *Polymer*, **46**, 9348–9361.
26 Grabowski, S.J. (2004) Hydrogen bonding strength—measures based on geometric and topological parameters. *J. Phys. Org. Chem.*, **17**, 18–31.
27 Skrovanek, D.J., Howe, S.E., Painter, P.C., and Coleman, M.M. (1985) Hydrogen bonding in polymers: infrared temperature studies of an amorphous polyamide. *Macromolecules*, **18**, 1676–1683.
28 Wang, L., Wang, Z., Zhang, X., Shen, J., Chi, L., and Fuchs, H. (1997) A new approach for the fabrication of an alternating multilayer film of poly(4-vinylpyridine) and poly(acrylic acid) based on hydrogen bonding. *Macromol. Rapid Commun.*, **18**, 509–514.
29 Chu, P.P. and Wu, H.D. (2000) Solid state NMR studies of hydrogen bonding network formation of novolac type phenolic resin and poly(ethylene oxide) blend. *Polymer*, **41**, 101–109.
30 Jiao, H., Goh, S.H., and Valiyaveettil, S. (2001) Mesomorphic interpolymer complexes and blends based on poly(4-vinylpyridine)–dodecylbenzenesulfonic acid complex and poly(acrylic acid) or poly(*p*-vinylphenol). *Macromolecules*, **34**, 7162–7165.
31 Kuo, S.W. and Chang, F.C. (2001) The study of miscibility and hydrogen bonding in blends of phenolics with poly (ε-caprolactone). *Macromol. Chem. Phys.*, **202**, 3112–3119.
32 Noda, I. (1989) Two-dimensional infrared spectroscopy. *J. Am. Chem. Soc.*, **111**, 8116–8118.
33 Noda, I. (2006) Progress in two-dimensional (2D) correlation spectroscopy. *J. Mol. Struct.*, **799**, 2–15.
34 Sun, B., Lin, Y., Wu, P., and Siesler, H.W. (2008) A FTIR and 2D-IR spectroscopic study on the microdynamics phase separation mechanism of the poly (*N*-isopropylacrylamide) aqueous solution. *Macromolecules*, **41**, 1512–1520.
35 Kuo, S.W. (2008) Effect of copolymer compositions on the miscibility behavior and specific interactions of poly (styrene-*co*-vinyl phenol)/poly (vinyl phenyl ketone) blends. *Polymer*, **49**, 4420–4426.
36 Noda, I. and Ozaki, Y. (2004) *Two-Dimensional Correlation Spectroscopy: Applications in Vibrational and Optical Spectroscopy*, John Wiley & Sons, Ltd, Chichester.
37 Huang, M.W., Kuo, S.W., Wu, H.D., Chang, F.C., and Fang, S.Y. (2002) Miscibility and hydrogen bonding in blends of poly (vinyl acetate) with phenolic resin. *Polymer*, **43**, 2479–2487.
38 Caravatti, P., Neuenschwander, P., and Ernst, R.R. (1986) Charcterization of polymer blends by selective proton spin-diffusion NMR measurements. *Macromolecules*, **19**, 1889–1895.
39 Wang, J., Cheung, M.K., and Mi, Y. (2001) Miscibility in blends of poly (4-vinylpyridine)/poly (4-vinylphenol) as studied by ^{13}C solid-state NMR. *Polymer*, **42**, 3087–3093.
40 Wang, J., Cheung, M.K., and Mi, Y. (2002) Miscibility and morphology in crystalline/amorphous blends of poly(caprolactone)/poly(4-vinylphenol) as studied by DSC, FTIR, and ^{13}C solid state NMR. *Polymer*, **43**, 1357–1364.

2

Hydrogen Bonding in Polymer Blends

Polymer blends feature two or more polymers combined together; they often have mechanical, thermal, and optoelectronic properties superior to those of their individual polymers. For economical and practical purposes, the most convenient and effective way to prepare new functional polymers is through a polymer blend approach using commercially available polymers, taking advantage of their high versatility and flexibility, rather than synthesizing a new material. Polymer blends can be classified into three basic phase behaviors: (i) completely miscible, (ii) immiscible, and (iii) partially miscible blend systems (Figure 2.1). Unfortunately, most polymer blend systems are usually incompatible and immiscible, meaning that their final products have properties inferior to those of the individual polymers. Controlling interfacial tension is critical in these compatible polymer blend systems to ensure obtaining desired blend morphologies and related physical properties. Decreasing interfacial tension and decreasing the sizes of the dispersed phase are the most important factors affecting the physical properties; most research activities related to polymer compatibilization in polymer blend systems have aimed at obtaining uniform physical properties. Using block or graft copolymers as efficient compatibilizers can lead to decreased interfacial tension and suppressed coalescence of the dispersed domains of polymer blends. Nevertheless, microphase separation can occur with most block copolymers, resulting in high viscosity and difficulty dispersing them into polymer blend systems, which might also prefer to form micelle structures at higher block copolymer concentrations. To overcome the problems associated with using block copolymers as compatibilizers, reactive compatibilization for incompatible polymer blends has been investigated widely during the past two decades. The main advantage of a reactive compatibilizer is the ability to suppress the coalescence of the dispersed domains significantly in a polymer blend system, using covalent bonds to stabilize the interface.

Figure 2.2 presents selected scanning electron microscopy (SEM) micrographs of a PA6/PBT = 30/70 blend containing various contents of compatibilizer [1]. Disperse spherical particle size and the phase contrasts for all blending system were decreased upon increasing the quantity of the compatibilizer. The epoxy functional group of the compatibilizer was indeed an efficient compatibilization agent, suppressing the phase coalescence with a smaller domain size based on the morphological transformation. An effective compatibilizer can enhance the

Hydrogen Bonding in Polymer Materials, First Edition. Shiao-Wei Kuo.

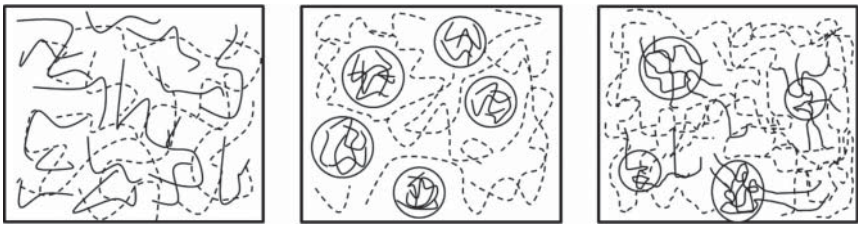

Figure 2.1 Typical morphologies of polymer blends classified as (a) miscible, (b) immiscible, and (c) partially miscible.

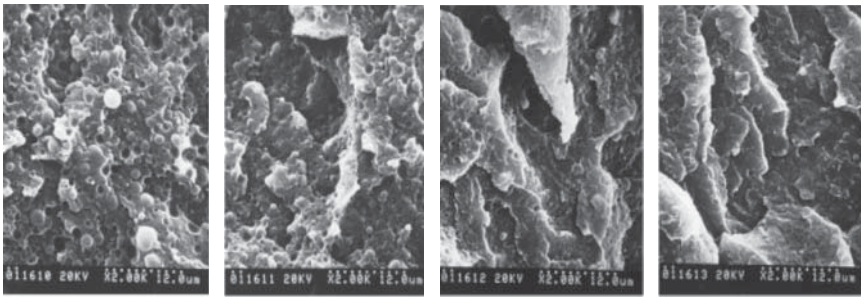

Figure 2.2 SEM images of PA/PBT = 30/70 in the presence of various concentrations: (a) 0, (b) 0.1, (c) 0.3, and (d) 0.5 phr for epoxy-functionalized compatibilizers [1]. (Chiou and Chang 2000 [1]. Reprinted with permission from John Wiley & Sons).

interfacial adhesion of a polymer blend system and, thus, improve its physical properties.

Nevertheless, compatible polymer blend systems remain immiscible, based on thermodynamic viewpoints, because most polymer blend systems have relatively high degrees of polymerization (DPs) and, thus, the favorable entropy terms of mixing become small relative to those of low-molecular-weight compound mixtures. Improving miscibility behavior in polymer blends is strongly dependent on the contribution of the enthalpic term; generally, it requires installing favorable intermolecular interactions (e.g., H-bonding, dipole–dipole, and π–π interactions) in the system. Many studies of polymer blends in recent years have involved intermolecular H-bonding. The miscibility of polymer blends; their self-assembly and supramolecular nanostructures; their nanocomposites; and low-surface-energy materials have all been investigated in detail in response to H-bonding strength. This chapter discusses each of these applications.

2.1 Thermodynamic Properties of Polymer Blends

In his book *Principles of Polymer Chemistry*, Flory recognized that miscible or single-phase polymer blends were a rare thing in 1953 [2]. Indeed, only

a few miscible polymer blend systems were reported at that time and it has becomes obvious, however, that many miscible polymer blend systems have been prepared from appropriate polymer pairs during the past four decades. These miscible polymer blend systems are generally those that feature functional groups capable of forming H-bonds. Painter and Coleman established their association model (PCAM) to describe these H-bonded miscible polymer blends; they added an additional term for the formation of H-bond interactions to modify the classical Flory–Huggins lattice theory for the Gibbs free energy (Equation 2.1) [3–5]:

$$\frac{\Delta G_{\mathrm{N}}}{RT} = \frac{\phi_1}{N_1}\ln\Phi_1 + \frac{\phi_2}{N_2}\ln\Phi_2 + \phi_1\phi_2\chi_{12} + \frac{\Delta G_{\mathrm{H}}}{RT} \tag{2.1}$$

where ϕ_i is the volume fraction of each polymer, N_i is the DP of each polymer, χ_{12} is the Flory–Huggins interaction parameter between polymers 1 and 2, and ΔG_{H} represents the free energy change arising from the formation of H-bonds in a polymer blend system. Simply speaking, the free energy in this equation is dependent on two major factors: the number of the H-bonds formed and the relative interassociation H-bonding strength in the blend system.

To understand the PCAM, we turn our attention to the classical Flory–Huggins lattice model. Flory independently proposed the first thermodynamic description of polymer mixture systems [2]:

$$\frac{\Delta G_{\mathrm{N}}}{RT} = \frac{\phi_1}{N_1}\ln\phi_1 + \frac{\phi_2}{N_2}\ln\phi_2 + \phi_1\phi_2 c_{12} \tag{2.2}$$

Differentiation of Equation 2.2 leads to the chemical potential:

$$\frac{\Delta u_1^0}{RT} = \ln\phi_1 + \left(1 - \frac{1}{r_2}\right)\phi_2 + \chi_{12}\phi_2^2 \tag{2.3}$$

where r_2 is the ratio of V_2/V_1 and

$$\chi'_{12} = \frac{\chi_{12}}{V_1} = \frac{z\Delta w_{12} r_1}{k_{\mathrm{B}} T V_1} \tag{2.4}$$

where z is the lattice coordination number and Δw_{12} is the energy change due to formation of the contact pairs between 1 and 2:

$$\Delta w_{12} = w_{12} - (w_{11} + w_{22})/2 \tag{2.5}$$

Here, χ_{12} is considered to be independent of concentration; it is predicted by Equation 2.4 to increase with pressure, but decrease with temperature. The term χ'_{12} is purely enthalpic, measured in terms of the difference in solubility parameters in the original treatment:

$$\chi'_{12} = \frac{(\delta_1 - \delta_2)^2}{RT} > 0 \tag{2.6}$$

Equation 2.2 has two shortcomings: it is not suitable for lower critical solution temperature (LCST) phase diagrams and it cannot predict polymer miscibility behavior arising from H-bonding interactions. During the past 30 years, many

scientists have modified the classical Flory–Huggins lattice theory, including the statistical thermodynamic analysis of polymer blends by Sanchez and Stone [6], the binary interaction model of Paul and Merfeld [7], and the association model of Painter and Coleman [8]. In general, the PCAM can predict the behavior of H-bonded polymer blends for most systems.

2.2 Association Model Approach

The association model was employed for many years to represent the behavior of mixtures of simple hydrocarbons and alcohols. As mentioned, Painter and Coleman appended an additional term to the classical Flory–Huggins lattice theory to account for the free energy of formation of H-bonds, as in Equation 2.2. Here, we use a simple example of the hydroxyl (OH) group to describe the character of this approach.

A compound containing an OH group (e.g., a phenol derivative) can form H-bonds from only its one OH functional group. The self-association equilibrium equation is described as [3]

$$B_1 + B_1 \overset{K_2}{\longleftrightarrow} B_2 \tag{2.7}$$

$$B_h + B_1 \overset{K_B}{\longleftrightarrow} B_{h+1} \quad (h > 2) \tag{2.8}$$

where K_2 or K_B can be described as

$$K_2 = \frac{\Phi_{B_2}}{2\Phi_{B_1}^2} \tag{2.9}$$

$$K_B = \frac{\Phi_{B_{h+1}}}{\Phi_{B_h}\Phi_{B_1}} \frac{h}{h+1} \tag{2.10}$$

For the competing equilibrium between A and B:

$$B_h + A_1 \overset{K_A}{\longleftrightarrow} B_hA \tag{2.11}$$

If the A unit sees no difference in H-bonding to the dimer or h-mers, then we have

$$K_A = \frac{\Phi_{B_hA}}{\Phi_{B_h}\Phi_{A_1}} \frac{hr}{h+r} \tag{2.12}$$

where K_2 and K_B are self-association equilibrium constants for the H-bonded dimer and h-multimers of the OH group (B), respectively; K_A is the interassociation equilibrium constant among H-bonded acceptor units (A) with the OH unit (B_h); r is the segmental molar volume ratio (V_A/V_B); and Φ_{B_h} and Φ_{A1} are the volume fractions of h-mers from OH groups (B) and H-bonded donor groups (A), respectively. The stoichiometric relationships are obtained simply on the basis of the consideration of materials balance. The total volume fractions for A and B